Volume 9 | Number 48 | 28 December 2018 | Pages 8897–9028

Chemical Science

rsc.li/chemical-science

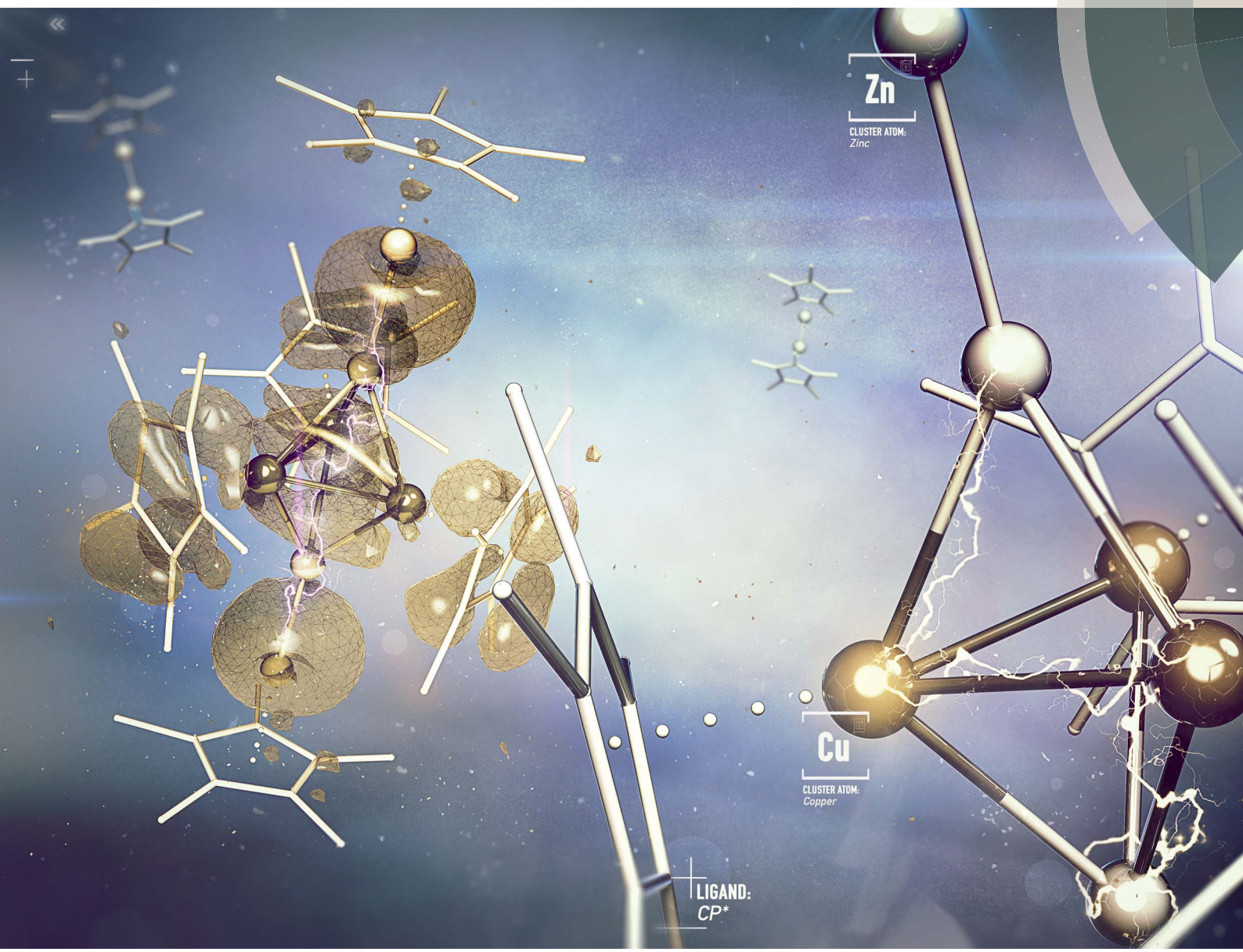

ISSN 2041-6539

ROYAL SOCIETY OF CHEMISTRY

EDGE ARTICLE

Jean-Yves Saillard, Roland A. Fischer *et al.*

Embryonic brass: pseudo two electron Cu/Zn clusters

Chemical Science

EDGE ARTICLE

View Article Online
View Journal | View Issue

Cite this: *Chem. Sci.*, 2018, **9**, 8906

All publication charges for this article have been paid for by the Royal Society of Chemistry

Embryonic brass: pseudo two electron Cu/Zn clusters†

Hung Banh,‡[ab] Julius Hornung,‡[ab] Thilo Kratz,[ab] Christian Gemel,[ab] Alexander Pöthig,[ab] Franck Gam,[c] Samia Kahlal,[c] Jean-Yves Saillard*[c] and Roland A. Fischer*[ab]

The isoelectronic M_7 clusters $[Cu_3Zn_4](Cp^*)_5$ (**1**) and $\{[Cu_2Zn_5](Cp^*)_5\}^+$ (**2**) are described. While **1** can be isolated only as a minor side product from the reaction of $Cu(CH_3CO_2)$ with equimolar amounts of $[Zn_2Cp^*_2]$ with the trigonal cluster $[CuZn_2](Cp^*)_3$ as the major product, **2** is available in acceptable yields from the reaction of $[CuZn_2](Cp^*)_3$ with the Cp^*Zn_2-transfer-reagent $[Cp^*Zn_2(Et_2O)_3][BAr_4^F]$. The trigonal bipyramidal Cu/Zn-clusters exhibit exceptional bonding situations: with formally only one skeleton electron pair they can be regarded as highly electron deficient. However, a detailed DFT analysis reveals that the cluster bonding is supported by 3d orbital contributions of the trigonal metal base unit. The data contribute to the development of an advanced tool-box for synthesis of Hume-Rothery intermetallic (*e.g.* brass) inspired clusters.

Received 1st September 2018
Accepted 26th October 2018

DOI: 10.1039/c8sc03902j

rsc.li/chemical-science

Introduction

Ligand stabilized metal clusters $[M_n](L)_m$ are fascinating links between molecules and bulk metals. They have attracted persistent interest since Hieber described $[Co_4](CO)_{12}$ [1] in 1932 up to the discovery of very high nuclearity transition-metal carbonyl clusters such as Dahl's $[Pd_{145}](CO)_{60}(PEt_3)_{30}$ [2] reported in 2000 and finally the thiolate-capped atom-precise gold clusters with the giant $[Au_{246}](p\text{-}MDT)_{80}$ [3] as a spectacular and recent example (2016).

A related break-through in main group metal clusters was Schnöckel's work on bottom-up synthesis based on metastable solutions of low valent group-13 species, and $[Al_{50}]Cp^*_{12}$ [4] (2004) became an icon of this chemistry ($Cp^* = C_5(CH_3)_5$). The cluster growth reactions are difficult to control and each case is very subtly dependent on the kinetic balance of many interlinked processes, *i.e.* disproportionation, agglomeration, ligand substitution and/or salt metathesis. Nevertheless, over the years a rich library of small, medium to high nuclearity clusters was successively developed.[5] In this context we started out to investigate the related organometallic cluster chemistry of Zn and studied the activation of low valent $[Zn_2Cp^*_2]$ by oxidative cleavage of one Zn–Cp* bond to induce disproportionation of the initial intermediate $[Zn_2Cp^*]^+$. From the reaction mixture $\{[Zn_{10}]Cp^*_6(CH_3)\}^+$ was isolated as the very first example of a ligated oligonuclear Zn-cluster.[6]

The synthetic scenario becomes even more diverse and challenging for bimetallic clusters $[M^1_aM^2_b](L)_m$, in particular when combining chemically distinctly different metals. A specific tool-box of suitable building blocks and reactions needs to be developed for each metal combination. For example, $[Cu_4Zn_4](CN^tBu)_4Cp^*_4$ is reproducibly available in moderate yields from $[Zn_2Cp^*_2]$ and $CpCu(CN^tBu)$ among other side products.[7] Reaction steps are the reduction of Cu(I) by Zn(I) under formation of $[Cp_2Zn]$, $[Cp^*CpZn]$ and $[Cp^*_2Zn]$ by involving Zn–Zn bond cleavage as well as Cp transfer from Cu to Zn as a side reaction. The $[M^1_aM^2_b]$ cores of such bimetallic clusters often mimic structural cut-outs from of the respective M^1/M^2 intermetallic solid-state phases.[8] Thus, the M_8-core of $[Cu_4Zn_4](CN^tBu)_4Cp^*_4$ is linked to an embryonic state of γ-brass, the classic Hume-Rothery intermetallic compound.

A rational design of the synthesis procedure to yield a specific Cu/Zn-cluster also requires knowledge of potentially preferred stability islands of "magic" compositions including the role of the capping ligands. While the electronic structures of classic transition metal carbonyl-clusters are often consistent with the Wade–Mingos rules originally developed for borane clusters, the electronic situation in metal clusters in general is more complicated and needs to be addressed by computational methods in every single case.[9] For example, the electron deficiency of $\{[Zn_{10}](Cp^*)_6(CH_3)\}^+$ results mainly from the fact that Zn can behave flexible in participating to cluster skeletal

[a]*Inorganic and Metalorganic Chemistry, Technical University Munich, Lichtenbergstr. 4, 85748 Garching bei München, Germany. E-mail: Roland.Fischer@tum.de*

[b]*Catalysis Research Center & Department of Chemistry, Technical University Munich, Ernst-Otto-Fischer-Str. 1, 85747 Garching bei München, Germany*

[c]*Univ Rennes, CNRS, ISCR-UMR 6226, F-35000 Rennes, France. E-mail: jean-yves.saillard@univ-rennes1.fr*

† Electronic supplementary information (ESI) available: CCDC 1854851 and 1854852. For ESI and crystallographic data in CIF or other electronic format see DOI: 10.1039/c8sc03902j

‡ Hung Banh and Julius Hornung equally contributed to this work.

bonding, sometimes providing one frontier orbital (like Group 11 metals) and sometimes providing three frontier orbitals (like Group 13 elements).[6,10] Following this research guidelines towards a library of oligonuclear Cu/Zn-clusters as embryonic brass species we report here on two astonishing cases. At a first glance they completely disobey the Wade–Mingos rules for deltahedral clusters. The two isoelectronic, trigonal bipyramidal M_7 clusters, namely the neutral $[Cu_3Zn_4]Cp^*_5$ (**1**) and the cation $\{[Cu_2Zn_5]Cp^*_5\}^+$ (**2**) are teaching us an interesting lesson.

Results and discussion

Synthesis and characterization of $[Cu_3Zn_4](Cp^*)_5$ (1)

Reaction of $Cu(CH_3CO_2)$ with equimolar amounts of $[Zn_2Cp^*_2]$ [11–13] in benzene at room temperature for three days leads to the formation of a dark red suspension of a mixture of unsoluble $Zn(CH_3CO_2)_2$, the known cluster $[CuZn_2](Cp^*)_3$ and the novel cluster $[Cu_3Zn_4](Cp^*)_5$ (**1**) as soluble components (Scheme 1).

From the filtered and concentrated reaction solution, $[CuZn_2](Cp^*)_3$ deposits as the main product in the form of yellow crystals at 8 °C in 57% isolated yield (based on Cp*). Further workup of the remaining solution gives $[Cu_3Zn_4](Cp^*)_5$ (**1**) co-crystallizing together with $[CuZn_2](Cp^*)_3$ at −30 °C in THF in form of dark red crystals. The single crystals of **1** could be isolated by manual separation from $[CuZn_2](Cp^*)_3$ with the aid of an optical microscope in a glove box under argon atmosphere. It should be noted, that we were not successful in increasing the yield of **1** by the change of reaction parameters such as time, temperature or stoichiometric ratio of the reactants. A more rational approach by using Cp^*Zn_2-transfer reagents similar to the synthesis of **2** (*vide infra*), is not possible in this case due to the inexistence of the required base unit $[Cu_3](Cp^*)_3$ (no skeleton bonding electrons). The formation mechanism of **1** is yet not clear. However, redox-reactions between Zn(I) and Cu(I) must play a role. While in the formation of the main product $[Zn_2Cu](Cp^*)_3$ from $Cu(CH_3CO_2)$ and $[Zn_2Cp^*_2]$ no redox-chemistry but only Cp* transfer reactions are involved, formation of **1** requires the reduction of M(I) to M(0). The accompanying oxidation process is obviously the formation of $Zn(CH_3CO_2)_2$ from the Zn(I) source.

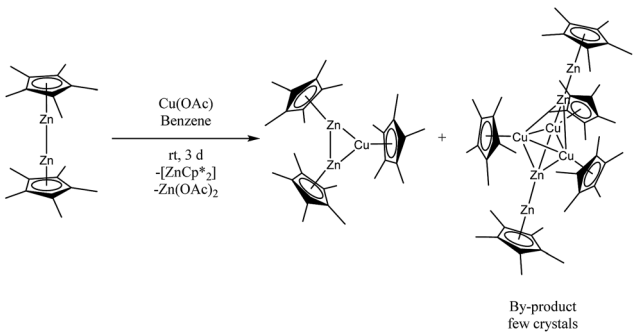

Scheme 1 Synthesis of $[CuZn_2]Cp^*_3$ and $[Cu_3Zn_4]Cp^*_5$ (**1**).

In situ ^{1}H NMR spectroscopy of the reaction mixture indicates rather clean formation of $[CuZn_2](Cp^*)_3$ under complete consumption of $[Zn_2Cp^*_2]$ (Fig. S4†) with $[Cp^*_2Zn]$ and **1** as minor by-products. An unidentified Cp*-containing intermediate can be detected, which almost completely disappears in the course of the reaction. The mechanism involves Cp* transfer from Zn to Cu as well as disproportionation of Zn(I) to Zn(0) and Zn(II). The identity of $[CuZn_2](Cp^*)_3$ has been confirmed by single crystal XRD measurement as well as NMR spectroscopic analysis. The data are in good agreement with the data reported in literature.[14] The separated single crystals of $[Cu_3Zn_4](Cp^*)_5$ (**1**) are stable under inert gas atmosphere for several months at −30 °C and are fairly soluble in non-polar solvents like *n*-hexane and benzene, but **1** dissolves very well in toluene, THF or fluorobenzene. However, it readily decomposes in solution at room temperature within a few hours under precipitation of metallic particles. This property limits further characterization of its reactivity.

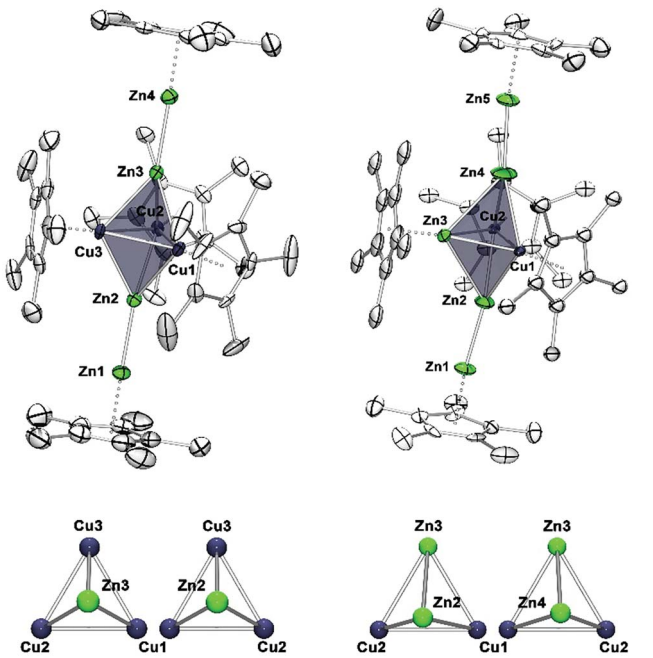

Fig. 1 Molecular structure of $[Cu_3Zn_4](Cp^*)_5$ (**1**) (left) and $\{[Cu_2Zn_5](Cp^*)_5\}^+$ (**2**) (right). The trigonal bipyramids are highlighted. Orthogonal view on the Cu1, Cu2, Cu3 plane showing the Cu1, Cu2, Cu3, Zn3/2 tetrahedrons of **1** (bottom, left). Orthogonal view on the Cu1, Cu2, Zn3 plane showing the Cu1, Cu2, Zn3, Zn2/4 tetrahedrons of **2** (bottom, right). Displacement ellipsoids are shown at the 50% probability level, the hydrogen atoms and disorders are omitted for clarity. Selected interatomic distances [Å] and angles [°] for **1**: Zn1–Zn2 = 2.318(2), Zn3–Zn4 = 2.317(2), Cu1–Cu2 = 2.446(2), Cu2–Cu3 = 2.431(2), Cu1–Cu3 = 2.442(2), Zn1–$Cp^*_{centr.}$ = 1.901, Zn4–$Cp^*_{centr.}$ = 1.922; Cu1–$Cp^*_{centr.}$ = 1.828; Cu2–$Cp^*_{centr.}$ = 1.827; Cu3–$Cp^*_{centr.}$ = 1.827; Cu3–Cu1–Cu2 = 59.65(5), Cu3–Cu2–Cu1 = 60.10(6), Zn2–Zn1–$Cp^*_{centr.}$ = 175.74, Zn3–Zn4–$Cp^*_{centr.}$ = 176.00. Selected interatomic distances [Å] and angles [°] for **2**: Zn1–Zn2 = 2.299(6), Zn4–Zn5 = 2.323(6), Cu1–Cu2 = 2.415(3), Cu1–Zn3 = 2.400(4), Zn3–Zn4 = 2.688(7), Cu1–Zn4 = 2.527(6), Cu2–Zn4 = 2.446(6); Cu1–Zn3–Cu2 = 60.47(9), Cu2–Cu1–Zn3 = 59.68(9), Zn3–Cu2–Cu1 = 59.85(10), Zn2–Zn1–$Cp^*_{centr.}$ = 174.62, Zn4–Zn5–$Cp^*_{centr.}$ = 172.05.

Compound **1** crystallizes in the monoclinic space group *Pn* with four distinct molecules in the asymmetric unit. Fig. 1 (left) shows only one of the four crystallographically distinct units for clarity. Note that Cu and Zn are not easily distinguishable by standard X-ray techniques, thus the assignment of Cu and Zn in the structure refinement has been supported by spectroscopic data (*vide infra*). The metal atoms are arranged in a trigonal bipyramidal fashion, with the apical positions occupied by ZnZnCp* units and the remaining equatorial triangle by CuCp* groups. Trigonal Cu_3 units are rather common in molecular clusters. However, in all species known the Cu–Cu contacts are supported by μ_2/μ_3-bridging and chelating ligands and are not bridged by other metal atoms as it is the case for **1**.[15–18] The Cu–Cp*$_{centr.}$ distances of **1** range from 1.827–1.828 Å and are shorter than the respective distances in the terminal Zn1–Cp*$_{centr.}$ (1.901 Å) and Zn4–Cp*$_{centr.}$ (1.922 Å) units.

However, all values are in good agreement to literature known Zn–Cp*$_{centr.}$ (1.83–2.19 Å) and Cu–Cp*$_{centr.}$ (1.82–1.96 Å) distances. The Zn1–Zn2 and Zn4–Zn5 bond lengths are almost identical with 2.318(2) and 2.317(2) Å, respectively. These values are well comparable to the Zn–Zn distance in $[Cp^*Zn_2(THF)_3]^+$ (2.317(7) Å) (Fig. S12†). All other M–M distances are distinctively longer with a narrow range of 2.431(2) (Cu1–Zn3)–2.458(2) Å (Cu2–Zn3). These data are similar to the Cu–Cu distance in $[Cu_4Zn_4](CN^tBu)_4(Cp^*)_4$ (2.471(4) Å)[7] and the average Zn–Zn distance in $\{[Zn_3](Cp^*)_3\}^+$ (2.430 Å), but elongated compared to the Zn–Cu distances (2.381(1) Å) of $[CuZn_2](Cp^*)_3$.[6,19] As a consequence, the trigonal bipyramid consists of two almost perfect $[Cu_3Zn]$ tetrahedrons sharing one trigonal Cu_3 face. Accordingly, the angles within the Cu1–Cu2–Cu3 triangle are all very close to 60° (59.65(5) for Cu3–Cu1–Cu2 and 60.25(6)° for Cu2–Cu3–Cu1). The Zn2–Zn1–Cp*$_{centr.}$ and Zn3–Zn4–Cp*$_{centr.}$ moieties are slightly deviated from linearity with angles of 175,74 and 176.00°, respectively.

Liquid injection field desorption mass spectrometry (LIFDI-MS) confirms the molecular composition of **1** with a well detectable $[M]^{\bullet+}$ ion peak at *m*/*z* [a.u.] = 1128 (Fig. 2) as well as two fragment peaks $[M–ZnCp^*]^{\bullet+}$ and $[M–ZnZnCp^*]^{\bullet+}$ at *m*/*z* [a.u.] = 927 and 861, respectively (Fig. S3†). Interestingly, no loss of CuCp* is observed in the fragment ions, confirming the assignment of elements in the X-ray single crystal structure with equatorial CuCp* and apical ZnZnCp* units.

The ^{1}H NMR spectrum of **1** in C_6D_6 at room temperature shows two Cp* resonances at 2.08 and 2.19 ppm in a 45 : 30 integral ratio, corresponding to the three chemically equivalent CuCp* groups as well as two equivalent apical ZnZnCp* groups. Accordingly, the ^{13}C NMR spectrum shows the expected set of signals for two different Cp* moieties (δ = 10.90 (s, $CuC_5\mathit{Me}_5$), 12.17 (s, $ZnZnC_5\mathit{Me}_5$), 104.62 (s, CuC_5Me_5), 110.18 (s, $ZnZnC_5Me_5$) ppm). Note, that the only assignment of metal atoms which is in agreement with this observed D_{3h} symmetry of the cluster in solution is the allocation of the four Zn atoms to the apical positions and the three Cu atoms to the equatorial triangle (Scheme S1†).

Synthesis and characterization of $\{[Cu_2Zn_5](Cp^*)_5\}[BAr_4^F]$ (**2**[BAr_4^F])

The reaction of $[Zn_2Cu](Cp^*)_3$ with two equivalents of the Cp^*Zn_2 transfer-reagent $[Zn_2(Cp^*)(Et_2O)_3][BAr_4^F]$[20] in fluorobenzene at room temperature for 1.5 h (Scheme 2) gives a dark red solution with very little amount of metallic precipitate. The product cluster $\{[Zn_5Cu_2](Cp^*)_5\}[BAr_4^F]\cdot 5C_6H_5F$ (**2**[BAr_4^F]$\cdot 5C_6H_5F$) crystallizes from the concentrated an filtered reaction solution at −30 °C in the form of dark red needles.

Minor amounts of an unidentified side product are removed by repeated recrystallization of the crude product in fluorobenzene at −30 °C giving **2**[BAr_4^F] in 23% analytically pure yield (based on Cu). As described for the formation of **1**, the reaction leading to **2** proceeds *via* a Cp* exchange mechanism. This is in nice accordance with the reactivity studies of $[Cp^*Zn_2(THF)_3]^+$ showing that this cation can act as both, a Cp* donor as well as a Cp* acceptor forming $\{[Zn_2](THF)_6\}^{2+}$ or $[Zn_2Cp^*_2]$ (Scheme S4†).[6] Likewise, an *in situ* NMR experiment of a mixture of $[Cp^*Zn_2(Et_2O)_3]^+$ and $[CuZn_2](Cp^*)_3$ at room temperature in fluorobenzene points to a rapid Cp* exchange between the metal atoms, indicated by the detection of only one coalescence signal for all Cp* groups. This signal decoalesces into two peaks at temperatures below −20 °C (see Fig. S7†). Due to incomplete separation of the signals at −50 °C, no integral ratio of the two peaks could be determined. As in the case of **1**,

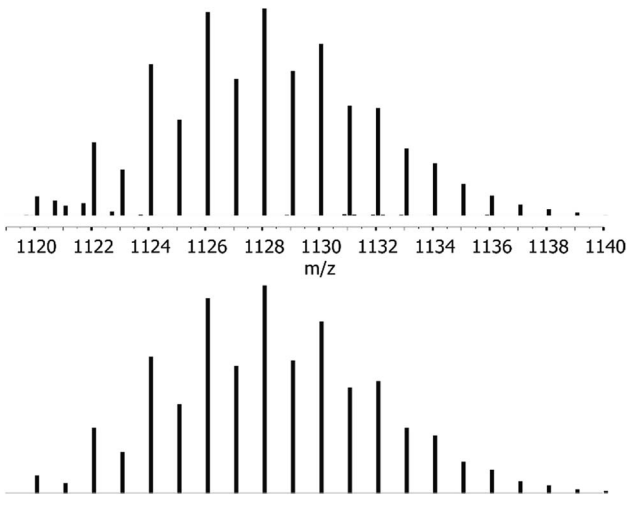

Fig. 2 Molecular ion peak of **1** (*m*/*z* = 1128) from LIFDI-MS measurements (top) and calculated isotopic pattern for **1** (bottom).

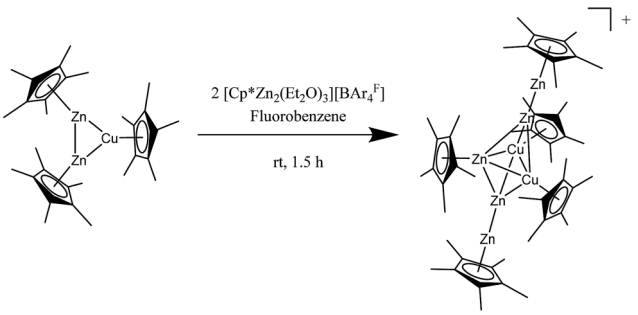

Scheme 2 Synthesis of $[Zn_5Cu_2]Cp^*_5[BAr_4^F]$ (**2**[BAr_4^F]).

changing reaction parameters such as temperature, time or stoichiometric ratio of the reactants did not result in any increase of the isolated yield. The complete pathway leading from the reactants to cluster **2** appears rather complex, as evident from the composition of the central trigonal M_3 unit. While the product exhibits a $[Cu_2Zn]$ central unit, the starting cluster consists of a $[CuZn_2]$ triangle. However, despite the obviously involved redox chemistry, no oxidized side products as it is the case in the synthesis of **1** could be detected.

The compound $\mathbf{2}[BAr_4^F]\cdot 5C_6H_5F$ crystallizes in the monoclinic space group *Cc* with two distinct ion pairs in the asymmetric unit. Only one of these two independent units is shown in Fig. 1 (above) for clarity. Similar to compound **1**, the metal atoms of cation **2** are arranged in a trigonal bipyramidal fashion, however, with higher deviations from the ideal polyhedral structure. Again, assignment of metal atoms to the atomic positions in the crystal structure has been done with the support of spectroscopic data (*vide infra*). The equatorial triangle consists of a Cu_2Zn unit capped by ZnZnCp* units on both sides. The apical Zn1–Zn2 (2.299(6) Å) and Zn4–Zn5 (2.323(6) Å) bond lengths are comparable to the respective apical Zn1–Zn2 (2.318(2) Å) and Zn3–Zn4 (2.317(2) Å) distances in **1**. The Cu1–Cu2 bond length in **2** (2.415(3) Å) is shorter than the Cu–Cu distances in $[Cu_4Zn_4](CN^tBu)_4Cp^*_4$ (2.471(4) Å) and in **1** (2.431(2)–2.446(2) Å).[7] The equatorial Cu_2Zn triangle is almost perfectly equilateral (Cu1–Cu2 = 2.415(3), Cu1–Zn3 = 2.400(4), Cu2–Zn3 = 2.396(3) Å). However, the intersection of the apical Zn2–Zn4 axis does not coincide with the centre of gravity of the equatorial Cu_3-plane, but is rather dislocated towards the Cu_2 edge. Thus, the contacts of the apical Zn atoms are not equidistant to the three equatorial metal atoms: the Zn3–Zn2 (2.745(6) Å) and Zn3–Zn4 (2.688(7) Å) distances are considerably longer than the Cu–Zn2 (avg. 2.463 Å) and Cu–Zn4 (avg. 2.487 Å) distances.

The molecular composition of $\mathbf{2}[BAr_4^F]$ as determined by EA (C, H) and AAS (Zn, Cu, B, F) is in good agreement with the sum formula (calculated for $H_{87}BC_{82}F_{24}Cu_2Zn_5$ [%]: H 4.40, B 0.54, C 49.41, F 22.87, Cu 6.38, Zn 16.40; found: H 4.62, B 0.47, C 51.48, F 20.20, Cu 6.48, Zn 15.98). The deviations in the carbon and fluorine values are attributed to the thermal instability of the compound and the difficulty in handling the pure samples. The ^{1}H NMR spectrum of $\mathbf{2}[BAr_4^F]$ in CD_2Cl_2 at room temperature shows three resonances at 1.96 (s, 30, $ZnZnC_5Me_5$), 2.04 (s, 15H, ZnC_5Me_5) and 2.12 (s, 30H, CuC_5Me_5) ppm for the three chemically non-equivalent Cp* groups in a 2 : 1 : 2 ratio, which points to a C_{2v} symmetry of **2** in solution. In addition, the expected set of signals for the $[BAr_4^F]^-$ anion 7.56 (s, 4H) and 7.72 ppm (s, 8H) are detected. Due to the high lability of $\mathbf{2}[BAr_4^F]$ in solution and the moderate solubility of $\mathbf{2}[BAr_4^F]$ at low temperatures meaningful ^{13}C NMR spectra could not be obtained. The IR spectrum reveals typical absorption bands for the Cp* moieties at 2905 and 2860 cm^{-1} and the C–F vibration of the $[BAr_4^F]^-$ anion at 1272 cm^{-1}.[20] The only reasonable assignment of elements to the metal core of the molecular structure of **2**, which is in agreement with the symmetry of the cation in solution (C_{2v}), is the allocation of four Zn atoms in the axial MMCp* moieties, leaving a $[ZnCu_2]$ triangle in the equatorial plane (Scheme S2†).

Cluster bonding analysis of 1 and 2

The polyhedral structure types of clusters are strongly related to their electronic structure, associating specific cluster shapes with specific numbers of electrons.[21–25] Stable closed-shell organometallic clusters (*e.g.* protected by hydrocarbon ligands *via* metal–carbon bonds) most often obey the Wade–Mingos electron-counting rules.[23–25] These rules state that the number of skeletal electron pairs (SEPs) associated with cluster bonding is equal to the number of vertices of the deltahedron in which the cluster is inscribed, plus one. Accordingly, the trigonal bipyramidal skeletons of **1** and **2**, should be associated with 5 + 1 = 6 SEPs. Cluster **1** can be formally considered as constituted of five fragments, three CuCp* and two Zn–ZnCp* units. Assuming first that, as generally admitted, the Cu and Zn 3d electrons are not significantly involved in the bonding, CuCp* and Zn–ZnCp* are 0- and 1-electron donor moieties, respectively. One thus ends up with only 1 SEP for **1**, as for its isoelectronic relative **2**. This makes **1** and **2** highly electron-deficient with respect to the Wade–Mingos rules. It should be however kept in mind that these rules assume that the fragments constituting the cluster participate to cluster bonding with 3 frontier orbitals, one of σ-type and two of π-type.[23–25] This is obviously the case for the Zn–ZnCp* moiety, the external Zn atom having two available non-bonding $4p_\pi$ frontier orbitals as well as one 4s/4p hybrid of σ-type (the other sp hybrid is involved in the Zn–Zn single bond). On the other hand, the case of the CuCp* (or $[ZnCp^*]^+$) fragment is different since it is generally considered as participating to the bonding with only one frontier orbital of σ-type (a 4s/4p hybrid), the occupied low-lying 3d-block being, as said above, discarded. Thus, the Wade–Mingos standard "reference" should be considered with caution when dealing with **1** and **2**. To clear out this situation, we have performed density functional (DFT) calculations on these two clusters as well as on several cluster models (BP86/STO-TZ2P level with Grimme D3BJ dispersion corrections, see Computational details in the ESI†). For the sake of simplicity we have first replaced the pentamethylcyclopentadienyl (Cp*) ligands in **1** and **2** by simple cyclopentadienyls (Cp). The optimized structures of the resulting models, namely **1′** and **2′**, were found to be energy minima for C_s symmetry, with their symmetry plane containing the Cu_3 and $ZnCu_2$ triangle, respectively. The optimized metrical data of **1′** and **2′** (Table 1) are consistent with their experimental counterparts in **1** and **2**. The $[Cu_3Zn_4]$ metal core of **1′** is very close to D_{3h} symmetry. Its Kohn–Sham orbital diagram is shown in Fig. 3.

The large HOMO–LUMO gap is consistent with the stability of **1**. In order to get a better insight into its bonding, a Morokuma–Ziegler energy decomposition analysis (EDA)[26–28] was carried out, considering the interaction between two fragments: A $\{[Cu_3](Cp)_3\}^{2-}$ triangular unit and a bi-capping $[CpZn_2\cdots Zn_2Cp]^{2+}$ "dimeric" unit. The formal fragment charges were chosen for closed-shell simplicity and also considering that $\{[Cu_3](Cp)_3\}^{2-}$ is isostructural and isoelectronic to the known $[CuZn_2](Cp^*)_3$ (see above),[14] which can be viewed as an isolobal[29,30] analogue of $[H_3]^+$ (σ-aromatic 2-electron/3-center bonding). A similar fragmentation has been suggested for the

Table 1 Selected averaged experimental (X-ray) and optimized (DFT) distances for **1**, **1′**, **2** and **2′** (in Å). The corresponding averaged computed Wiberg indices are given in parenthesis for **1′** and **2′**. The Zn′ and Zn″ labels designate the zinc atom bonded to Cp*/Cp and that belonging to the Cu_2Zn triangle in **2′**, respectively

(avg)	**1** (X-ray)	**1′** (DFT)	**1** (DFT)
Cu–Cu	2.440	2.414 (0.270)	2.426
Cu–Zn	2.443	2.470 (0.091)	2.432
Zn–Zn′	2.318	2.345 (0.600)	2.314
(avg)	**2** (X-ray)	**2′** (DFT)	**2** (DFT)
Cu–Cu	2.417	2.385 (0.339)	2.401
Cu–Zn	2.475	2.490 (0.074)	2.437
Cu–Zn″	2.399	2.399 (0.268)	2.401
Zn–Zn′	2.311	2.338 (0.606)	2.299
Zn–Zn″	2.717	2.872 (0.025)	2.682

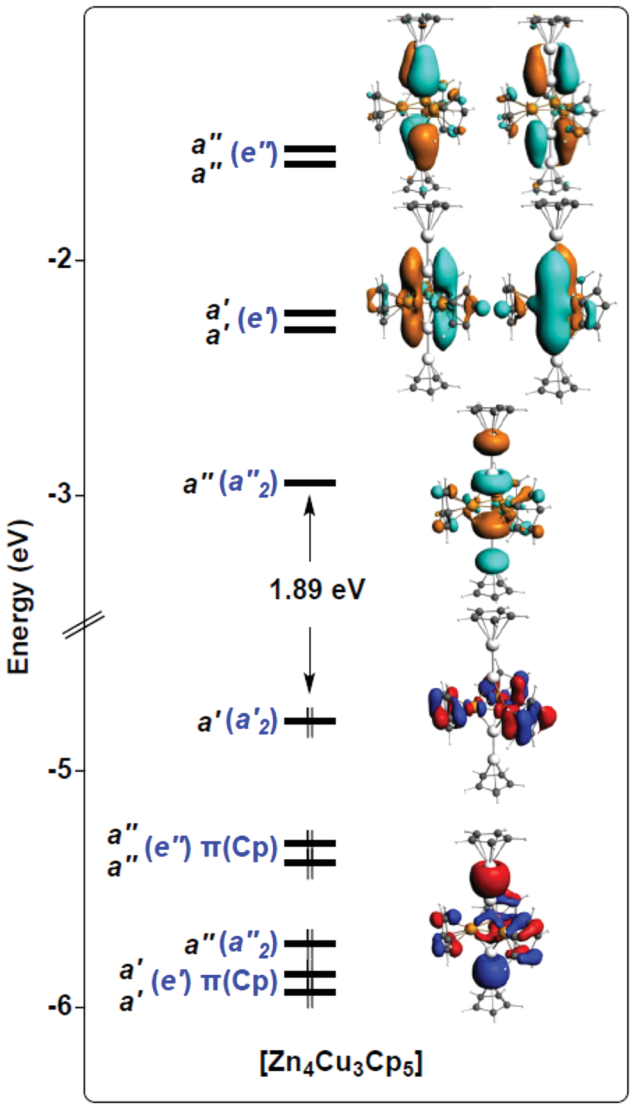

Fig. 3 Kohn–Sham orbital diagram of $[Cu_3Zn_4](Cp)_5$ (**1′**). The levels are labelled according to C_s symmetry (in black) and D_{3h} pseudo-symmetry (in blue). The C_s symmetry plane contains the Cu_3 triangle.

cluster $[\{Pd(C_6H_4F)\}_3(\mu_2\text{-}SC_6H_4Cl)_3Ag(H_2O)_2][BF_4]_2$ implying that an aromatic $[Pd_3]^+$ triangle acts as a donor ligand to a Ag^+ ion.[31] The same approach has also been used for treating a related $[Pd_4]^{2+}$ system.[32] The EDA results are given in Table 2.

Unsurprisingly, with such a formal fragment partitioning in **1′**, the electrostatic interaction component dominates the total bonding energy. Representing 44% of the former, the orbital interaction component is, however, not negligible. Its a′ and a″ components, respectively of σ- and π-type with respect to the Cu_3 plane, are of similar order, the a′ interaction being the strongest. A detailed analysis of the **1′** Kohn–Sham orbital compositions based on its fragment orbitals allowed us to describe the covalent component of the bonding interaction through the simplified qualitative interaction orbital diagram sketched in Fig. 4, considering D_{3h} pseudo-symmetry.

The $[CpZn_2\cdots Zn_2Cp]^{2+}$ "dimer" has six accepting frontier orbitals, the in-phase and out-of-phase combinations of the three accepting orbitals on the terminal Zn of each $[CpZn_2]^+$ "monomer" (see above). In the D_{3h} pseudo-symmetry of **1′**, the sp(Zn) hybrids give rise to a'_1 and a''_2 combinations, whereas the $4p_\pi$(Zn) AO's lead to e′ and e″ combinations (see left side of Fig. 4). On the other hand, the $\{[Cu_3](Cp)_3\}^{2-}$ unit has no accepting orbitals. Its highest occupied levels are the π(Cp) and 3d(Cu) combinations, among which is buried the strongly bonding a'_1 orbital, principally of 4s/4p composition, which contains the 3-center bonding electron pair of this fragment. This Cu_3 a'_1 orbital interacts strongly with the a'_1 LUMO of the $[CpZn_2\cdots Zn_2Cp]^{2+}$ "dimeric" fragment, giving rise to a fully in-phase, strongly bonding, combination which contains the unique SEP that one would consider for cluster bonding if no 3d(Cu) orbitals were involved (see above).

But in fact 3d(Cu) combinations of proper symmetry interact with the other accepting orbitals of the $[CpZn_2\cdots Zn_2Cp]^{2+}$ fragment. This can be traced by the occupation of it's a''_2, e′ and e″ frontier orbitals, which is 0.54, 2 × 0.10 and 2 × 0.11, respectively. For comparison, the a'_1 occupation is 1.02. The 3d(Cu) counterparts are of $3d_\pi$ (a''_2 and e″) and $3d_{z^2}$ (e′) character. Counting the resulting bonding pairs, one ends up with 6 SEPs, all of the proper symmetry (a'_1, a''_2, e′ and e″) as in clusters satisfying the classical Wade–Mingos rules. Thus, to some extent, **1** satisfies the Wade–Mingos rules, despite not all, but only specific, $3d_\pi$ and $33d_{z^2}$ combinations are involved. Moreover, the e′ and e″ interactions are not very strong, because of the relatively poor energy match between 4p(Zn) and 3d(Cu). On the other hand, some second-order participation to the bonding (not represented in Fig. 4) and involving the a_1' and a''_2 combinations associated with the Zn–Zn bonding pairs can also be traced. This tends to weaken somewhat the strength of the Zn–Zn bonds at the expenses of Zn–Cu bonding, as exemplified by the computed Zn–Zn Wiberg index in **1′** (0.600), significantly weaker than in CpZnZnCp (0.811).

To summarize the above MO analysis, the bonding within the $[Cu_3Zn_2]$ trigonal bipyramidal skeleton in **1** can be viewed as intermediate between that of a hypothetical electron-deficient 1-SEP cluster and that of a regular Wade–Mingos 6-SEP species. It should be pointed out that, although not preponderant, the role of the $4p_\pi$(Zn) AOs in the framework stability is

Table 2 Morokuma–Ziegler energy decomposition analysis (EDA) of **1′** and **2′**. All values in eV. E_{Pauli} = Pauli repulsion; E_{elstat} = electrostatic interaction; E_{orb} = orbital interaction. TBE = total bonding energy = $E_{Pauli} + E_{elstat} + E_{orb} + E_{disp}$

	1′ (C_s)		**2′** (C_s)	
Fragments	$[Cu_3Cp_3]^{2-} + [CpZn_2\cdots Zn_2Cp]^{2+}$		$[Cu_2ZnCp_3]^{-} + [CpZn_2\cdots Zn_2Cp]^{2+}$	
E_{Pauli}	14.92		10.37	
E_{elstat}	−24.53		−14.15	
$E_{orb,decomposition}$	a′	−6.30	a′	−4.30
	a″	−4.55	a″	−3.48
E_{orb}	−10.85		−7.78	
E_{disp}	−1.24		−1.16	
TBE	−21.70		−12.72	

crucial. This can be shown by replacing in **1′** the $[CpZnZn]^+$ capping units by $[CpZn]^+$ fragments which, assuming η^5-Cp coordination, do not possess $4p_\pi$ accepting frontier orbitals. Indeed, the optimized geometry of the resulting M_5 cluster $[Cu_3Zn_2](Cp)_5$ (see ESI†) exhibits (η^1-Cp)Zn units, rather than (η^5-Cp)Zn, thus leaving the $4p_\pi$(Zn) orbitals available for bonding within the $[Zn_2Cu_3]$ trigonal bipyramidal skeleton. With such a low coordination mode associated with the rather fragile electron-poor character of the $[Cu_3Zn_2]$ skeleton, the hypothetical $[Cu_3Zn_2](Cp)_5$ cluster appears unlikely to be isolable.

The optimized structure of the model **2′** is also in good agreement with the X-ray structure of **2** (see Table 1). In particular it shows a rather long Zn(apical)–Zn″(equatorial) bond of 2.872 Å. It is noteworthy that when the dispersion corrections are not included in the calculations, the Zn–Zn″ distance is elongated to 3.019 Å, a no-bond value. Thus, despite the small E_{disp} component in the fragment energy decomposition of Table 2, the dispersion forces appear to play a significant role in the overall cluster structure. The weak covalent Zn–Zn″ bonding is also exemplified by its low Wiberg index (0.025). It can be explained by the fact that the highest 3d-type combinations of the $\{[Cu_2Zn](Cp)_3\}^-$ fragment have little Zn participation (3d(Zn) levels are lower) and therefore interact with the $4p_\pi$(Zn) combinations of the $[CpZn_2\cdots Zn_2Cp]^{2+}$ "dimer" primarily through the copper atoms.

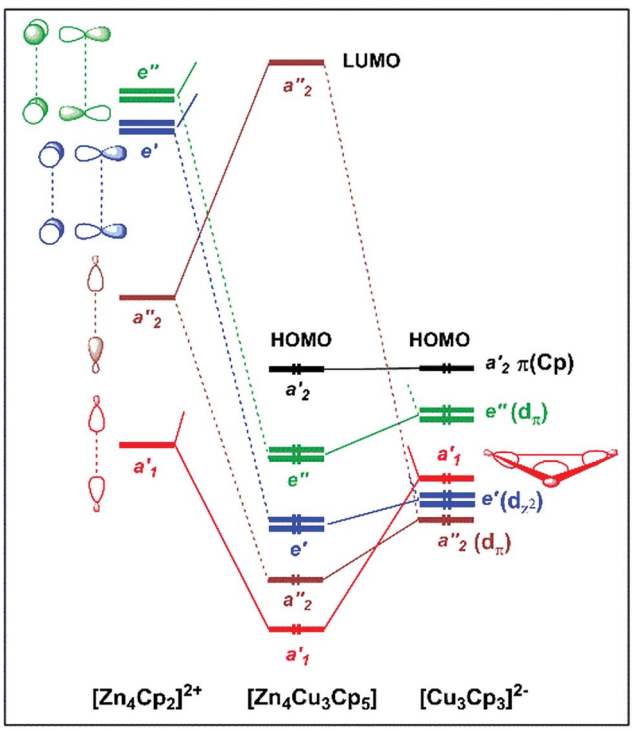

Fig. 4 Simplified orbital diagram describing the interaction of the $[Cu_3Cp_3]^{2-}$ and $[CpZn_2\cdots Zn2Cp]^{2+}$ fragments in **1′** (D_{3h} pseudo-symmetry assumed). The occupied 3d(Zn) and (most of) the 3d(Cu) combinations, not involved in the interaction, are not represented.

The structures of the real methylated compounds **1** and **2** were also optimized and were found to be of C_1 symmetry, slightly distorted away from C_s due to the steric effect of the methyl groups. Their selected metrical data reported in Table 1 are in good agreement with that of the X-ray structures. For these compounds, it was not possible to perform a 2-fragment EDA analysis similar to that carried out for the **1′** and **2′** models. As a matter of fact, it was not possible to converge the $[Cp^*Zn_2\cdots Zn_2Cp^*]^{2+}$ unit in the proper closed-shell configuration. However, a 3-fragment analysis in which this "dimeric" unit is split into two $[Cp^*Zn_2]^+$ fragments was possible. The corresponding results, together with that obtained in a similar way for **1′** and **2′** are provided in Table S2.† It appears clearly that the 2- and 3-fragment EDA analyses of **1′** and **2′** are fully consistent and indicate negligible interaction between the two capping $[Cp^*Zn_2]^+$ units. Comparing in Table S2,† the results obtained for **1** and **2** with that of **1′** and **2′** indicate that the bonding analysis carried out for the non-methylated models applies to the real methylated compounds. Among the changes upon ligand methylation (*i.e.* Cp *vs.* Cp*), one can note an increase of the absolute value of the E_{orb} component by ∼1.6/1.8 eV due a destabilization of the $[Cu_3]$ or $[Cu_2Zn]$ 3d(Cu) block. The E_{disp} component is also doubled upon methylation, due to methyl⋯methyl van der Waals interactions. However, with an absolute value increase of ∼1.3/1.4 eV, its contribution to the total bonding interaction remains relatively small (7–10% of the sum of the stabilizing components).

Going back to the long Zn–Zn″ bond in **2** (exp: 2.717 Å, calc: 2.872 Å; averaged values), it is interesting to note that, within the series of pseudo-homoleptic $[TM(ZnR)_n]$ compounds (TM = d-block metal) the shortest intramolecular Zn–Zn contact was found to be 2.676(1) Å in $[Ru(ZnCp^*)_4(ZnMe)_6]$[33] being only slightly shorter than the corresponding contacts in **2**.

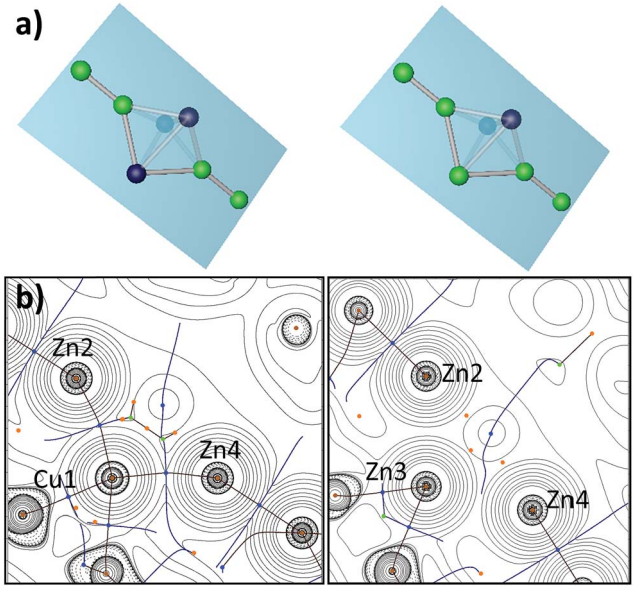

Fig. 5 (a) M_7 cluster unit of **1** (left) and **2** (right) showing the M_5 plane that was used for QTAIM analysis. (b) Contour line map of the Laplacian $\nabla^2\rho(r)$ of **1** in the plane containing Zn2, Cu1 and Zn4 (left) and of **2** in the plane containing Zn2, Zn3 and Zn4 (right). Solid lines indicate areas of charge concentration while dashed lines show area of charge depletion. The thick solid lines (brown) connecting the atomic nuclei are the bonds paths. The thick solid lines (blue) separating the atomic basins indicate the zero-flux surfaces crossing the molecular plane. Blue dots are (3,−1) bond critical points, orange dots (3,1) ring critical points and green dots (3,3) cage critical points.

Investigations of the bonding in these compounds revealed that the Zn–Zn interactions should not be interpreted as strong Zn–Zn covalent bonds but rather as weak Zn⋯Zn interactions. Therefore, the rather small Wiberg bond index of 0.16 found for the Zn3–Zn2/Zn3–Zn4 contacts in **2** can also be interpreted as rather weak interactions. In this respect a complementary view is obtained from Quantum Theory of Atoms in Molecules (QTAIM, see Computational details in the ESI†) analysis of **1** and **2**. Bond critical points and bond paths are found for all M–M interactions, except for the long Zn–Zn″ contacts in **2** (see Fig. 5 where they are labelled Zn3–Zn2 and Zn3–Zn4 as in the X-ray structures). In accordance to these observations, ring and cage critical points can be found for all M_3 triangles and M_4 pyramides in **1**, whereas in **2** ring critical points are only found for the Cu_2Zn triangles. Alternatively, especially cluster **2** can be viewed as a copper triple bonded moiety $[Cp^*CuCuCp^*]^{2-}$ (with occupied π-like orbitals),[34] which is "ligated" by three groups $[ZnR]^+$ (R = Cp*, ZnCp*). This picture is in accordance with the results of the QTAIM analysis, which suggests isolated $[ZnR]^+$ fragments (see ESI†).

Summary and perspectives

In summary, the homoleptic all-hydrocarbon Cp*-protected M_7 Cu/Zn-clusters $[Cu_3Zn_4](Cp^*)_5$ (**1**) and $\{[Cu_2Zn_5](Cp^*)_5\}^+$ (**2**) have been synthesized and characterized. They expand the unique series $\{[Cu_aZn_b](Cp^*)_c\}^{n+}$ with varying Cu/Zn ratios $a:b$ and Cp* content. The series starts with the M_3 clusters $\{[Zn_3](Cp^*)_3\}^+$ and $[CuZn_2](Cp^*)_3$, it includes the (heteroleptic) M_8 cluster $[Cu_4Zn_4](Cp^*)_4(CN^tBu)_4$. The series so far ends with the M_9 and M_{10} all-zinc clusters $[Zn_9](Cp^*)_6$ and $\{[Zn_{10}](Cp^*)_6(CH_3)\}^+$ (see the Introduction).[2–4] The new M_7 clusters **1** and **2** demonstrate the feasibility to substitute Zn and Cu on a molecular level in small nuclearity clusters while keeping the cluster's polyhedral structural type. As to that the preparation of further isoelectronic structural pairs of $\{[Cu_aZn_b](L)_c\}^{n+}$ ($a + b = 4$–6) and expanded versions of such clusters (*i.e.* with higher nuclearity $a + b > 10$), which only differ in the Zn : Cu ratio appears feasible. The trigonal bipyramidal clusters **1** and **2** are at first glance with 1 SEP highly electron deficient with regard to the Wade–Mingos rules, owing to the fact that the basal MCp* units lack 4p frontier orbitals. However, according to EDA analysis of the model **1′** based on the fragments $\{[Cu_3](Cp)_3\}^{2-}$ and $[CpZn_2\cdots Zn_2Cp]^{2+}$ not only 4s/p orbitals of the trigonal M_3 basal unit are involved in skeletal bonding, but even if to a lower extend, also $3d_\pi$ and $3d_{z^2}$ combinations. The latter provide frontier orbitals of proper symmetry and 5 additional SEPs to satisfy the Wade–Mingos rules for trigonal bipyramidal clusters. In spite of the fact that some of these additional SEPs have only moderate bonding character, the metal skeletons of **1** and **2** do not need the help of μ_2/μ_3 ligands for maintaining their unbridged bipyramidal trigonal structures. Dispersion interactions between the Cp* protecting ligands provide additional stabilization to the structures. This is a specific property of Cp* as a ligand,[19,35] among others such as its flexible coordination mode ($\eta^1\cdots\eta^5$), its transferability between Cu and Zn centres, its steric bulk and the stabilization of elimination products such as $[Cp^*_2Zn]$ (related to disproportionation reactions). It can be expected that other oligonuclear Cu/Zn clusters on the borderline between electron deficient and regular Wade–Mingos species are likely to be highly reactive and thus should allow further cluster expansion reactions, eventually reaching stability islands of larger clusters predicted by the superatom model. Our ultimate goal along these lines would be the demonstration of high nuclearity atom-precise Hume-Rothery intermetallics inspired superatom clusters solely protected by all-hydrocarbon ligands, such as the recently discovered M_{55} magic number Al/Cu cluster $[Cu_{43}Al_{12}](Cp^*)_{12}$.[35]

Conflicts of interest

There are no conflicts to declare.

Acknowledgements

This work was supported by the Deutsche Forschungsgemeinschaft (grant Fi-502/23-2). H. B. is grateful for a PhD scholarship donated by the German Chemical Industry Fund. We thank Prof. T. Marder and his co-workers at the Julius-Maximilians-Universität Würzburg and Linden CMS GmbH for support in mass spectrometry. The GENCI French national computer resource center is acknowledged (grant x2016-087367). F. G. thanks the Région Bretagne for a PhD studentship grant (ARED NANOCLU 9334).

Notes and references

1 W. Hieber, F. Mühlbauer and E. A. Ehmann, *Ber. Dtsch. Chem. Ges. A/B*, 1932, **65**, 1090–1101.
2 N. T. Tran, D. R. Powell and L. F. Dahl, *Angew. Chem., Int. Ed.*, 2000, **39**, 4121–4125.
3 C. Zeng, Y. Chen, K. Kirschbaum, K. J. Lambright and R. Jin, *Science*, 2016, **354**, 1580–1584.
4 J. Vollet, J. R. Hartig and H. Schnöckel, *Angew. Chem., Int. Ed.*, 2004, **43**, 3186–3189.
5 H. Schnöckel, *Chem. Rev.*, 2010, **110**, 4125–4163.
6 H. Banh, K. Dilchert, C. Schulz, C. Gemel, R. W. Seidel, R. Gautier, S. Kahlal, J.-Y. Saillard and R. A. Fischer, *Angew. Chem., Int. Ed.*, 2016, **55**, 3285–3289.
7 K. Freitag, H. Banh, C. Gemel, R. W. Seidel, S. Kahlal, J. Y. Saillard and R. A. Fischer, *Chem. Commun.*, 2014, **50**, 8681–8684.
8 K. Mayer, J. Weßing, T. F. Fässler and R. A. Fischer, *Angew. Chem., Int. Ed.*, 2018, **57**, 14372–14393.
9 T. Fehlner, J. F. Halet and J. Y. Saillard, *Molecular Clusters: A Bridge to Solid-State Chemistry*, Cambridge University Press, 2013.
10 K. Freitag, C. Gemel, P. Jerabek, I. M. Oppel, R. W. Seidel, G. Frenking, H. Banh, K. Dilchert and R. A. Fischer, *Angew. Chem., Int. Ed.*, 2015, **54**, 4370–4374.
11 I. Resa, E. Carmona, E. Gutierrez-Puebla and A. Monge, *Science*, 2004, **305**, 1136–1138.
12 M. Carrasco, R. Peloso, I. Resa, A. Rodriguez, L. Sanchez, E. Alvarez, C. Maya, R. Andreu, J. J. Calvente, A. Galindo and E. Carmona, *Inorg. Chem.*, 2011, **50**, 6361–6371.
13 M. Carrasco, R. Peloso, A. Rodriguez, E. Alvarez, C. Maya and E. Carmona, *Chem.–Eur. J.*, 2010, **16**, 9754–9757.
14 K. Freitag, C. Gemel, P. Jerabek, I. M. Oppel, R. W. Seidel, G. Frenking, H. Banh, K. Dilchert and R. A. Fischer, *Angew. Chem., Int. Ed.*, 2015, **54**, 4370–4374.
15 M. Zhang, B.-C. Su, C.-L. Li, Y. Shen, C.-K. Lam, X.-L. Feng and H.-Y. Chao, *J. Organomet. Chem.*, 2011, **696**, 2654–2659.
16 J. Li, J. M. White, R. J. Mulder, G. E. Reid, P. S. Donnelly and R. A. O'Hair, *Inorg. Chem.*, 2016, **55**, 9858–9868.
17 W.-Y. Lo, C.-H. Lam, V. W.-W. Yam, N. Zhu, K.-K. Cheung, S. Fathallah, S. Messaoudi, B. Le Guennic, S. Kahlal and J.-F. Halet, *J. Am. Chem. Soc.*, 2004, **126**, 7300–7310.
18 M. I. Bruce, J.-F. Halet, B. Le Guennic, B. W. Skelton, A. N. Sobolev, C. J. Sumby and A. H. White, *Coord. Chem. Rev.*, 2018, **375**, 2–12.
19 K. Freitag, H. Banh, C. Gemel, P. Jerabek, R. W. Seidel, G. Frenking and R. A. Fischer, *Inorg. Chem.*, 2015, **54**, 352–358.
20 K. Freitag, H. Banh, C. Ganesamoorthy, C. Gemel, R. W. Seidel and R. A. Fischer, *Dalton Trans.*, 2013, **42**, 10540–10544.
21 H. A. Jahn and E. Teller, *Proc. Roy. Soc. Lond. Math. Phys. Sci.*, 1937, **161**, 220.
22 A. C. Reber and S. N. Khanna, *Acc. Chem. Res.*, 2017, **50**, 255–263.
23 D. M. Mingos and D. J. Wales, in *Introduction to cluster chemistry*, Prentice-Hall, Englewood Cliffs, 1990.
24 D. M. P. Mingos, *Nat. Phys. Sci.*, 1972, **236**, 99–102.
25 K. Wade, in *Transition Metal Clusters*, ed. B. F. G. Johnhson, John Wiley & Sons, Chichester, 1980, pp. 193–264.
26 K. Morokuma, *J. Chem. Phys.*, 1971, **55**, 1236–1244.
27 T. Ziegler and A. Rauk, *Inorg. Chem.*, 1979, **18**, 1558–1565.
28 F. M. Bickelhaupt and E. J. Baerends, *J. Rev. Comput. Chem.*, Wiley, New York, 2000.
29 M. Elian, M. M. L. Chen, D. M. P. Mingos and R. Hoffmann, *Inorg. Chem.*, 1976, **15**, 1148–1155.
30 R. Hoffmann, *Angew. Chem., Int. Ed.*, 1982, **21**, 711–724.
31 Y. Wang, A. Monfredini, P. A. Deyris, F. Blanchard, E. Derat, G. Maestri and M. Malacria, *Chem. Sci.*, 2017, **8**, 7394–7402.
32 A. Muñoz-Castro, D. M.-L. Carey and R. Arratia-Pérez, *J. Chem. Phys.*, 2010, **132**, 164308.
33 T. Cadenbach, T. Bollermann, C. Gemel, M. Tombul, I. Fernandez, H. M. van, G. Frenking and R. A. Fischer, *J. Am. Chem. Soc.*, 2009, **131**, 16063–16077.
34 Y. Xie, H. F. Schaefer III and R. B. King, *J. Am. Chem. Soc.*, 2005, **127**, 2818–2819.
35 J. Wessing, C. Ganesamoorthy, S. Kahlal, R. Marchal, C. Gemel, O. Cador, A. C. H. Da Silva, J. L. F. Da Silva, J. Y. Saillard and R. A. Fischer, *Angew. Chem., Int. Ed.*, 2018, **57**, 14630–14634.